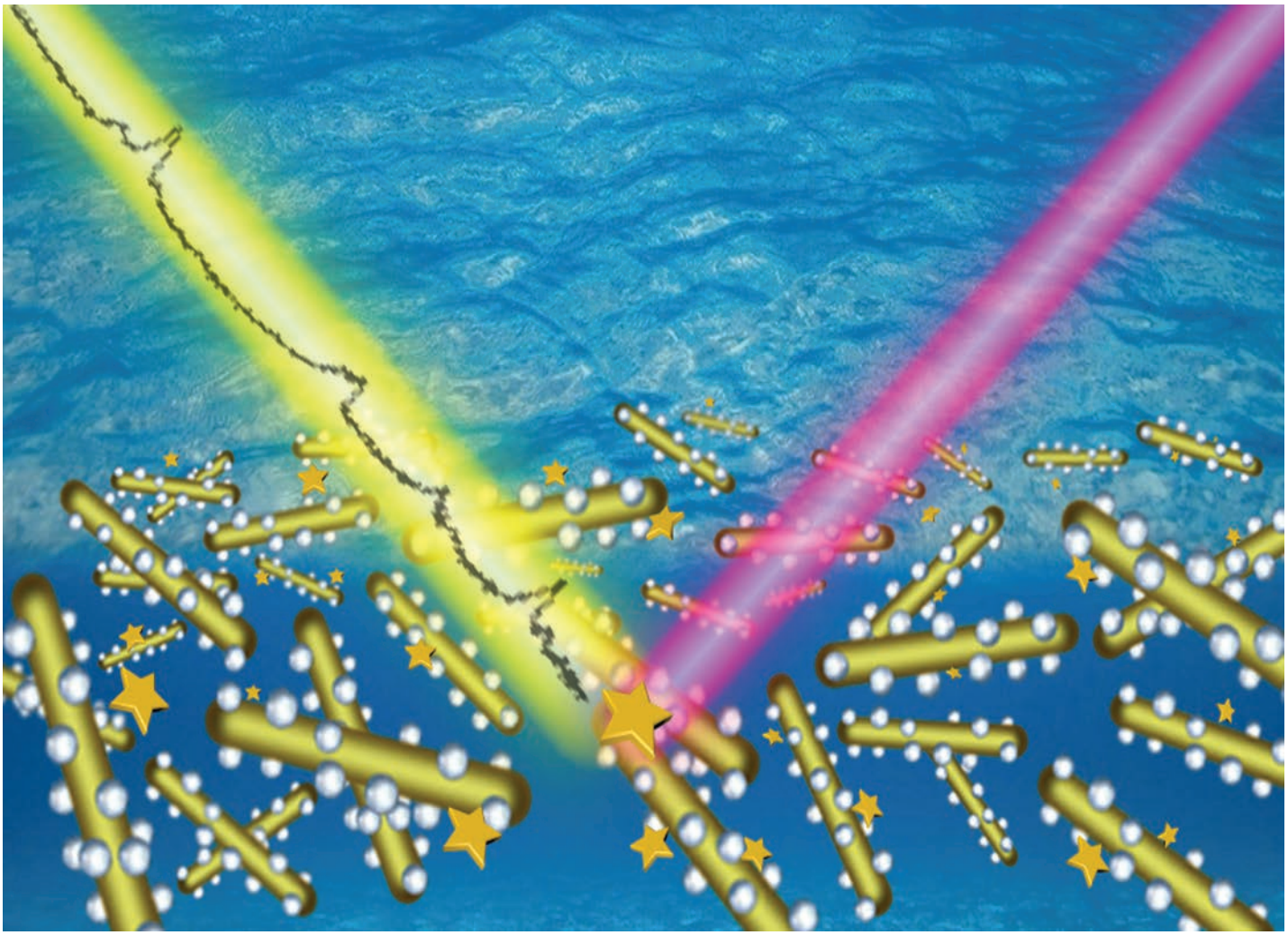

Showcasing research from Heyou Han Research Laboratory (Nano-Bioanalytic Laboratory), State Key Laboratory of Agricultural Microbiology, Huazhong Agricultural University, Wuhan, China.

Title: Universal chitosan-assisted synthesis of Ag-including heterostructured nanocrystals for label-free *in situ* SERS monitoring

A universal chitosan-assisted method was developed to synthesize various Ag-included heterostructured nanocrystals, in which chelation probably plays a vital role. The as-prepared Ag/Pd heterostructured nanocrystals show outstanding properties when being used as bifunctional nanocomposites in label-free *in situ* SERS monitoring of Pd-catalytic reaction.

As featured in:

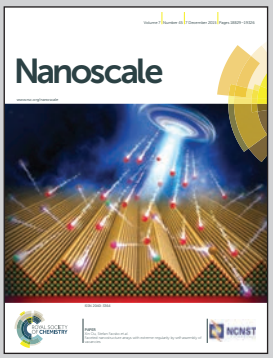

See Heyou Han *et al.* *Nanoscale*, 2015, **7**, 18878.

ROYAL SOCIETY OF CHEMISTRY

www.rsc.org/nanoscale

Registered charity number: 207890

Nanoscale

COMMUNICATION

View Article Online
View Journal | View Issue

Cite this: *Nanoscale*, 2015, **7**, 18878

Received 16th May 2015,
Accepted 3rd September 2015

DOI: 10.1039/c5nr03223g

www.rsc.org/nanoscale

Universal chitosan-assisted synthesis of Ag-including heterostructured nanocrystals for label-free *in situ* SERS monitoring†

Kai Cai,‡ Xiaoyan Xiao,‡ Huan Zhang, Zhicheng Lu, Jiawei Liu, Qin Li, Chen Liu, Mohamed F. Foda and Heyou Han*

A universal chitosan-assisted method was developed to synthesize various Ag-including heterostructured nanocrystals, in which chelation probably plays a vital role. The as-prepared Ag/Pd heterostructured nanocrystals show outstanding properties when used as bifunctional nanocomposites in label-free *in situ* SERS monitoring of Pd-catalyzed reaction.

Surface-enhanced Raman scattering (SERS) possesses inherent advantages in label-free *in situ* monitoring of the catalyzed reaction process, which can help in understanding the reaction mechanism and optimize the catalyst formula.[1–5] It is well known that some noble metal structures, such as Ag and Au nanocrystals, are required for magnifying the molecule information in the SERS process.[5–9] Moreover, SERS is a short-range effect, and the catalyzed reaction is a process taking place at the surface of the catalyst. Hence, assembling nanocrystals with SERS activity and the catalyst together is significant for realizing an accurate and highly effective monitoring.

Recently, various protocols for fabricating the bifunctional units, which combine both catalytic and SERS activities, have been developed for label-free *in situ* monitoring.[3,5,7,8,10–16] A general strategy to fabricate the units is to coat a SERS-active core with a catalytically active surface, including assembling small Au nanoparticles (NPs) on the core or coating the core with a shell of Pt or Pd.[4,5,10,11,17] However, it is difficult to achieve a balance between high catalytic efficiency and SERS enhancement in this method, as the plasmon of the core will be significantly decreased with the increase of shell thickness.[4,12,17]

In addition, other methods, such as depositing isolated Au NPs and Pt NPs simultaneously onto the glass substrate to study Pt-catalyzed reaction, provide a different route.[1] But the non-chemically bound metal nanoparticles are unpractical as a system under real catalytic conditions.[3] It is known that the Au core is the most employed material in the fabrication of bifunctional units, including Au nanorods and nanowires.[3–8,10,11,18–20] In fact, Ag has a stronger localized surface plasmon resonance (LSPR) and can provide a higher enhancement factor than Au even though the latter is more chemically inert, which is an advantage in assembling bifunctional structures.[17,21–23]

Heterogeneous metal nanocrystals (HMNCs) are common entities formed by integrating some metal nanocrystals of different compositions, which are jointed through permanent bonding interfaces.[24–29] Particularly, the oligomer-type HMNCs, which are different from the core–shell type ones, expose multiple material surfaces, which can avoid the dilemma in maintaining the balance between catalytic and SERS activities.

Pd and Pt are the most important catalysts used in many applications, including the conversion of chemical to electrical energy and a series of vital organic chemical reactions.[30,31] Therefore, it is highly desirable to synthesize oligomer-type HMNCs containing Ag and Pd (Pt) and use them as the substrate for the label-free *in situ* SERS monitoring.

Herein, we demonstrate a facile synthesis of Ag/Pd oligomer-type heterostructured nanotubes (OHNTs), in which some Ag NPs are jointed to one-dimensional (1D) Pd nanotubes (NTs) through permanent bonding interfaces. Chitosan plays a vital role in the successful preparation of Ag/Pd OHNTs; without chitosan, Ag could not heterogeneously nucleate and grow on the NTs uniformly. The method was then successfully used to grow Ag NPs on bimetallic NTs, such as PdPt alloy NTs or quasi-1D Au/PtAu heterojunction NTs. Finally, Ag/Pd OHNTs were used to monitor the reaction process of *p*-nitrothiophenol (*p*-NTP) to *p*-aminothiophenol (*p*-ATP) in label-free *in situ* by SERS in aqueous solution.

The Te nanowires (NWs) were synthesized at first. Then the Pd NTs were synthesized by using Te NWs as the template and chitosan as the stabilizing agent in aqueous solution at room temperature. The TEM images of the as-prepared Te NWs and

State Key Laboratory of Agriculture Microbiology, College of Food Science and Technology, College of Science, Huazhong Agricultural University, Wuhan 430070, China. E-mail: hyhan@hzau.edu.cn

†Electronic supplementary information (ESI) available. See DOI: 10.1039/c5nr03223g

‡Equal contribution.

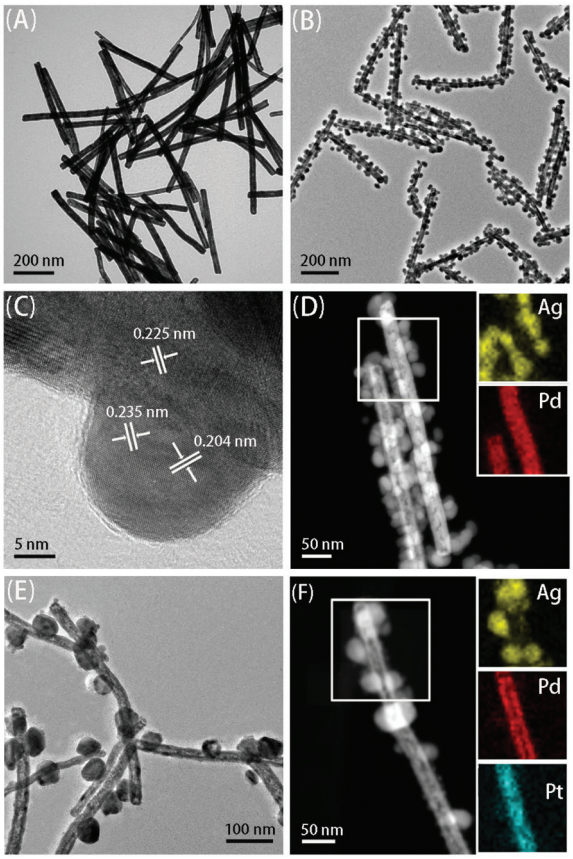

Fig. 1 TEM images of Pd NTs (A), Ag/Pd OHNTs (B), Ag/PdPt OHNTs (E). HRTEM images of Ag/Pd OHNTs (C). HAADF-STEM images of Ag/Pd OHNTs (D), Ag/PdPt OHNTs (F).

Pd NTs are shown in Fig. S1† and Fig. 1A, respectively. It is shown that Pd NTs have the same size as the Te NW template (about 30 nm in diameter and 420 nm in length), and it can be observed that the centers of the 1D Pd nanostructures are obviously brighter than the edges, suggesting that they are hollow nanotubes. The XRD pattern of the Pd NTs (Fig. S2†) shows a characteristic diffraction peak which can be assigned to the (111) lattice plane of face-centered-cubic (fcc) Pd structures. The other peaks of fcc Pd were not obviously observed, which might have been caused by a lack of other planes with an appropriate area.

Ag NPs grow on the Pd NTs by reducing silver nitrate with ascorbic acid in the chitosan and PVP solution. The typical TEM image of Ag/Pd OHNTs is shown in Fig. 1B. Some 0-dimensional (0D) nanocrystals with a diameter of 30 nm grow on the surface of 1D Pd NTs. The HRTEM image of Ag/Pd OHNTs (Fig. 1C) shows that the attached NPs are jointed to the Pd NTs through permanent bonding interfaces and a crystal boundary can be clearly observed. One of the interplanar spacings of the nanotube is about 0.225 nm, which is consistent with the (111) lattice plane of fcc Pd, and 0.235 and 0.204 nm in the particles are corresponding to the (111) and (200) lattice planes of fcc Ag, respectively. In addition, the high-angle annular dark-field scanning TEM-energy-dispersive X-ray spectroscopy (HAADF-STEM-EDS) elemental mapping image of the Ag/Pd OHNT shows the distinct compositional distribution of each constituent metal element (Fig. 1D). It unambiguously reveals that Ag NPs are linked to the 1D Pd NT skeleton. The energy-dispersive X-ray spectroscopy (EDS) performed on Pd NTs (Fig. S3†) shows that they are mainly composed of Pd and Ag elements. The presence of a few Te elements indicates that the used templates are Te NWs. When the amount of Pd precursors used in the synthesis of Pd NTs was adjusted, the Te elements could be completely absent. The XRD pattern of the Ag/Pd OHNTs (Fig. S2†) shows more characteristic diffraction peaks than the last one, which can be suitably assigned to the reflections from the fcc structure of Ag. When Pd and Pt precursors were added simultaneously instead of a single Pd precursor using the same method, PdPt bimetallic NTs were obtained (Fig. S4†). According to inductively coupled plasma atomic emission spectroscopy (ICP-AES) analysis, the molar ratio of Pd : Pt is about 7 : 1. The TEM images of the as-prepared Ag/PdPt OHNTs show that they have the same morphology with Ag/Pd OHNTs (Fig. 1E). Moreover, HAADF-STEM-EDS was used to further characterize the structure. As shown in Fig. 1F, Ag elements are distributed on NPs while both Pd and Pt elements are distributed on NTs, revealing that Ag NPs are linked to the 1D PdPt bimetallic NT skeleton. The EDS performed on Ag/PdPt OHNTs (Fig. S5†) shows that they are composed of Pd, Pt and Ag elements, but no Te element was observed.

In order to investigate the role of chitosan in the synthesis of heterostructured nanocrystals, a contrast test was performed. Porous PdPt NTs were synthesized using Te NWs as templates in hexadecyltrimethylammonium bromide (CTAB) solution, and were then used as the intermediate for the following synthesis (Fig. S6†). ICP-AES analysis shows that the molar ratio of Pd : Pt in the NTs is about 11 : 9. When chitosan was used as the surfactant, as shown in Fig. 2A, all of the Ag NPs are jointed on the porous PdPt NTs. In Fig. 2B, HAADF-STEM-EDS further demonstrates that the Ag NPs are jointed on the PdPt NTs, and the EDS analysis (Fig. S7†) shows that they are composed of Pd, Pt and Ag elements. However, when using polyvinyl pyrrolidone (PVP) as the surfactant instead of using chitosan, Ag NPs cannot grow uniformly on the surface of the porous PdPt NTs. A typical result is shown in Fig. 2C: Ag NPs tend to aggregate and are not well-distributed. To further understand the effect, we tested other surfactants in the synthesis instead of chitosan, such as CTAB, sodium dodecyl sulfate (SDS) and acrylic acid polymers (PAA) (Fig. S8†). Probably because of the electrostatic repulsion of CTAB and Ag ions or the termination of growth of little Ag NPs by CTAB, no Ag NPs appear clearly on the nanotubes. Even though SDS exhibits a negative charge and Ag ions can absorb on the nanotubes, not all Ag NPs are grown on the nanotubes. Moreover, PAA has the same performance as SDS because it also has a negative charge. Chitosan is a polysaccharide biopolymer formed by the deacetylation of the naturally occurring chitin with a large number of functional groups. Although it

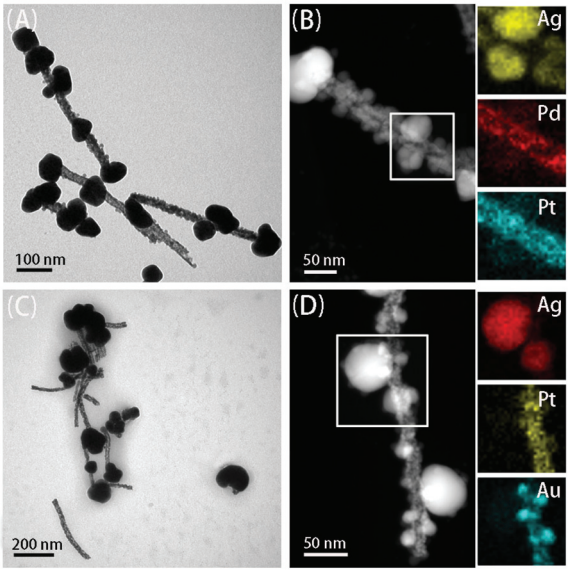

Fig. 2 TEM images of Ag/PdPt OHNTs using chitosan (A) and PVP (C) as surfactants in the synthesis. HAADF-STEM images of Ag/PdPt OHNTs (B) and Ag/Au/PtAu heterostructured nanotubes (D).

has a positive charge as CTAB, it possesses unique polycationic and chelating properties.[32,33] In this research, chelation induced the even dispersion of Ag ions on the surface of the metal NPs, which probably provides the essential conditions for the heterogeneous nucleation and growth of Ag on the NPs. In addition, adhesion may have a certain effect on the process. Therefore, we can conclude that chitosan plays a vital role in the preparation of Ag-including heterostructured nanocrystals.

In addition, to further confirm the method, a more complicated heterostructure, Au/PtAu heterostructured NTs, was used as the intermediate to fabricate Ag-including heteronanostructures. The Au/PtAu heterostructured NTs were prepared firstly (Fig. S9†), and were then used in the next process. The TEM image demonstrates that Ag-including heterostructures were obtained (Fig. S10†). HAADF-STEM-EDS was also used to test the result. As shown in Fig. 2D, Ag NPs are obviously linked to the surface of the PtAu NTs. The EDS performed on the structures shows that they are composed of Au, Pt and Ag elements (Fig. S11†). Even though Ag and Au crystals have a higher match than Ag and Pt crystals, in the presence of chitosan, it was not observed that more Ag NPs were linked to Au NPs than to PtAu NT frameworks as expected. When using PVP instead of chitosan in the synthesis, we found that Ag NPs apparently were not well-distributed on the surface of Au/PtAu heterostructured NTs (Fig. S12†). All these results demonstrate that chitosan is vital in the heterostructured growth of Ag NPs on other materials and the chitosan-assisted method is a universal strategy to obtain Ag-including heterostructures.

It is well known that many noble metal NPs can catalyze the reaction of *p*-NTP to *p*-ATP. Herein, UV-vis absorption spectra were used to testify the catalytic properties of the Ag/Pd heterostructured nanocrystals. As shown in Fig. 3, the absorption intensity of *p*-NTP at 410 nm wavelength decreases over time in the presence of the Ag/Pd heterostructured nanocrystals, while the contrast experiment shows no change (Fig. S13†). Obviously, the as-prepared Ag/Pd heterostructured nanocrystals have catalytic activity towards the reaction of *p*-NTP to *p*-ATP. This result is in conformity with the anticipation, as only a part of the surface of the Pd NTs is covered by Ag NPs and considerable Pd atoms are exposed to the solution. When the borohydride ions reacted with Pd, the electrons from the donor were relayed to the acceptor *p*-NTP right after both of them were absorbed onto the particle surfaces.

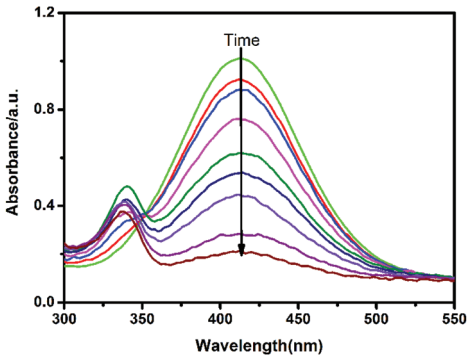

Fig. 3 Time dependent UV-vis absorption spectra for the reduction of *p*-NTP by $NaBH_4$ in the presence of Ag/Pd OHNTs. The absorption spectra were recorded every 3–4 min.

After the catalytic activity was determined, the SERS sensitivity was assessed. A series of Raman spectra were collected from the reaction system in sequence after the addition of $NaBH_4$. It is noteworthy that all samples were measured in aqueous solution without a special mixing process in our study, both of which are significant for a label-free *in situ* monitoring of the metal-catalyzed reaction process by recording the SERS response in real time. As shown in Fig. 4, four characteristic peaks at 1082, 1113, 1345 and 1572 cm^{-1} in the bottom spectra are clearly observed, which are in accordance with

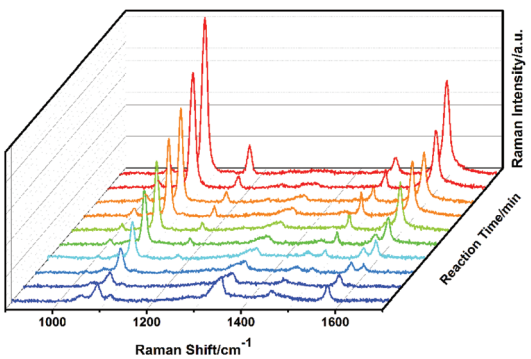

Fig. 4 SERS spectra recorded from the reaction suspension collected at different reaction times. From bottom to top: SERS spectra recorded at 0, 1, 2, 3, 4, 5, 6, 7, 8 and 12 min after addition of $NaBH_4$ solution.

those of pure *p*-NTPs. As time went on, the characteristic peaks at 1345 and 1572 cm^{-1}, which correspond to R-NO_2 of *p*-NTP, gradually decrease and finally disappear, while two new peaks at 1007 and 1590 cm^{-1}, which correspond to phenyl ring modes of *p*-ATP, were clearly observed. Generally, the intensity ratios of the peaks at 1572 and 1590 cm^{-1} were used to monitor the catalyzed reaction. From the nonexistence of the peak at 1590 cm^{-1} at the beginning to the final disappearance of the peak at 1572 cm^{-1}, the reaction process in the experiment was recorded by SERS monitoring (Fig. S14†). Because both the catalyzed reaction and SERS took place at the surface of nanocrystals, we directly measured the samples in aqueous solution without washing the *p*-NTP after a mixing process.

It is worth pointing out that no peaks of *p*,*p*′-dimercaptoazobenzene (DMAB), which usually emerge in the reaction by various catalysts, were observed in the process. Moreover, PdAg bimetallic nanofibers were used as the catalyst in the same reaction and the intermediate product was observed in the process.[17] However, the PdAg heterostructures produced a different result in this work, even though a high laser power was used, which usually assists the production of the photochemical product.[5,34] Xie *et al.* reported that the production of an intermediate product can be avoided by using a thin layer silica shell to isolate the inert Au core from the actual catalytic Au satellites.[7] Herein, we consider that the structural features of the catalyst are probably an important reason for the non-appearance of the reaction intermediate.

In conclusion, we have demonstrated a universal chitosan-assisted method for the facile synthesis of Ag-including heterostructured nanocrystals in aqueous solution at room temperature. Chitosan promotes the heterostructured nucleation and growth of Ag on other nanostructures in the synthesis. The as-prepared Ag/Pd heterostructured nanocrystals were used to monitor the reaction process of *p*-NTP to *p*-ATP by SERS in real time in aqueous solution successfully. The superior properties of the bifunctional nanocomposites exhibit great potential in label-free *in situ* SERS monitoring of Pd-catalyzed reaction. The design concept described here can also be extended to other bi- or tri-metallic NPs according to the actual requirement of the study on metal-catalyzed reaction *in situ* by SERS.

Acknowledgements

The authors acknowledge financial support from the National Natural Science Foundation of China (21375043, 21175051) and the Doctor Innovation Project of Huazhong Agricultural University (0900205179).

Notes and references

1 V. Joseph, C. Engelbrekt, J. Zhang, U. Gernert, J. Ulstrup and J. Kneipp, *Angew. Chem., Int. Ed.*, 2012, **51**, 7592.
2 D. Wu, L. Zhao, X. Liu, R. Huang, Y. Huang, B. Ren and Z. Tian, *Chem. Commun.*, 2011, **47**, 2520.
3 Q. Cui, A. Yashchenok, L. Zhang, L. Li, A. Masic, G. Wienskol, H. Möhwald and M. Bargheer, *ACS Appl. Mater. Interfaces*, 2014, **6**, 1999.
4 R. Liu, J.-F. Liu, Z.-M. Zhang, L.-Q. Zhang, J.-F. Sun, M.-T. Sun and G.-B. Jiang, *J. Phys. Chem. Lett.*, 2014, **5**, 969.
5 J. Huang, Y. Zhu, M. Lin, Q. Wang, L. Zhao, Y. Yang, K. X. Yao and Y. Han, *J. Am. Chem. Soc.*, 2013, **135**, 8552.
6 Y.-C. Tsao, S. Rej, C.-Y. Chiu and M. H. Huang, *J. Am. Chem. Soc.*, 2014, **136**, 396.
7 W. Xie, B. Walkenfort and S. Schlücker, *J. Am. Chem. Soc.*, 2013, **135**, 1657.
8 W. Xie, C. Herrmann, K. Kömpe, M. Haase and S. Schlücker, *J. Am. Chem. Soc.*, 2011, **133**, 19302.
9 R. A. Álvarez-Puebla, R. Contreras-Cáceres, I. Pastoriza-Santos, J. Pérez-Juste and L. M. Liz-Marzán, *Angew. Chem., Int. Ed.*, 2009, **48**, 138.
10 Z. Y. Bao, D. Y. Lei, R. Jiang, X. Liu, J. Dai, J. Wang, H. L. W. Chan and Y. H. Tsang, *Nanoscale*, 2014, **6**, 9063.
11 Q. Cui, G. Shen, X. Yan, L. Li, H. Möhwald and M. Bargheer, *ACS Appl. Mater. Interfaces*, 2014, **6**, 17075.
12 W. Cai, X. Tang, B. Sun and L. Yang, *Nanoscale*, 2014, **6**, 7954.
13 X. Tang, W. Cai, L. Yang and J. Liu, *Nanoscale*, 2014, **6**, 8612.
14 X. Liang, T. You, D. Liu, X. Lang, E. Tan, J. Shi, P. Yin and L. Guo, *Phys. Chem. Chem. Phys.*, 2015, **17**, 10176.
15 G. Zheng, L. Polavarapu, L. M. Liz-Marzán, I. Pastoriza-Santos and J. Pérez-Juste, *Chem. Commun.*, 2015, **51**, 4572.
16 D. Qi, X. Yan, L. Wang and J. Zhang, *Chem. Commun.*, 2015, **51**, 8813.
17 M. Cao, L. Zhou, X. Xu, S. Cheng, J.-L. Yao and L.-J. Fan, *J. Mater. Chem. A*, 2013, **1**, 8942.
18 Y. Wang, Y.-Q. Wang, B. Yan and L.-X. Chen, *Chem. Rev.*, 2013, **113**, 1391.
19 J.-R. Li, G.-G. Zhang, L.-H. Wang, A.-G. Shen and J.-M. Hu, *Talanta*, 2015, **140**, 204.
20 M. Lin, Y.-Q. Wang, X.-Y. Sun, W.-H. Wang and L.-X. Chen, *ACS Appl. Mater. Interfaces*, 2015, **7**, 7516.
21 T. Yang, H. Yang, S. J. Zhen and C. Z. Huang, *ACS Appl. Mater. Interfaces*, 2015, **7**, 1586.
22 M. Potara, A. Gabudean and S. Astilean, *J. Mater. Chem.*, 2011, **21**, 3625.
23 M. Potara, S. Boca, E. Licarete, A. Damert, M. Alupei, M. T. Chiriac, O. Popescu, U. Schmidt and S. Astilean, *Nanoscale*, 2013, **5**, 6013.
24 Y. Yu, Q. Zhang, Q. Yao, J. Xie and J. Y. Lee, *Acc. Chem. Res.*, 2014, **47**, 3530.
25 L. Carbone and P. D. Cozzoli, *Nano Today*, 2010, **5**, 449.
26 C. Wang, W. Tian, Y. Ding, Y.-q. Ma, Z. L. Wan, N. M. Markovic, V. R. Stamenkovic, H. Daimen and S. Sun, *J. Am. Chem. Soc.*, 2010, **132**, 6524.
27 J. Gu, Y.-W. Zhang and F. Tao, *Chem. Soc. Rev.*, 2012, **41**, 8050.
28 S. Mourdikoudis, M. Chirea, D. Zanaga, T. Altantzis, M. Mitrakas, S. Bals, L. M. Liz-Marzán, J. Pérez-Juste and I. Pastoriza-Santos, *Nanoscale*, 2015, **7**, 8739.

29 K. Cai, J. Liu, H. Zhang, Z. Huang, Z. Lu, M. F. Foda, T. Li and H. Han, *Chem. – Eur. J.*, 2015, **21**, 7556.
30 X. Xia, S.-I. Choi, J. A. Herron, N. Lu, J. Scaranto, H.-C. Peng, J. Wang, M. Mavrikakis, M. J. Kim and Y. Xia, *J. Am. Chem. Soc.*, 2013, **135**, 15706.
31 E. Antolini, *Energy Environ. Sci.*, 2009, **2**, 915.
32 H. Jiang, Z. Chen, H. Cao and Y. Huang, *Analyst*, 2012, **137**, 5560.
33 H. Yi, L.-Q. Wu, W. E. Bentley, R. Ghodssi, G. W. Rubloff, J. N. Culver and G. F. Payne, *Biomacromolecules*, 2005, **6**, 2881.
34 L.-B. Zhao, J.-L. Chen, M. Zhang, D.-Y. Wu and Z.-Q. Tian, *J. Phys. Chem. C*, 2015, **119**, 4949.